Influence of porosity on cavitation instability predictions for elastic–plastic solids

Viggo Tvergaard[a,*], Guadalupe Vadillo[b]

[a]Department of Mechanical Engineering, Solid Mechanics, Technical University of Denmark, Dk 2800 Kgs. Lyngby, Denmark
[b]Department of Continuum Mechanics and Structural Analysis, University Carlos III of Madrid, Avda. de la Universidad 30, 28911 Leganés, Madrid, Spain

Abstract

Cavitation instabilities have been found for a single void in a ductile metal stressed under high triaxiality conditions. Here, the possibility of unstable cavity growth is studied for a metal containing many voids. The central cavity is discretely represented, while the surrounding voids are represented by a porous ductile material model in terms of a field quantity that specifies the variation of the void volume fraction in the surrounding metal. As the central void grows, the surrounding void volume fractions increase in nonuniform fields, where the strains grow very large near the void surface, while the high stress levels are reached at some distance from the void, and the interaction of these stress and strain fields determines the porosity evolution. In some cases analysed, the porosity is present initially in the metal matrix, while in other cases voids nucleate gradually during the deformation process. It is found that interaction with the neighbouring voids reduces the critical stress for unstable cavity growth.

Keywords: Plasticity; Instability; Finite strains; Ductile fracture

1. Introduction

Cavitation instabilities have been predicted for a single void in an elastic–plastic solid, in cases where the stress levels are sufficiently high such that the work released in the field surrounding the expanding void is enough to drive continued expansion. Such high stress levels are typically reached in metal–ceramic systems, where the constraint on plastic flow in the metal leads to very high stress triaxialities. The unstable void growth has been studied by Bishop et al. [1] for spherically symmetric conditions, and similar cavitation instabilities have been found by Huang et al. [2] and Tvergaard et al. [3] for spherical voids subject to axisymmetric stress conditions, as long as the ratio of the transverse stress and the axial tensile stress is near unity. In related spherically symmetric studies for nonlinear elasticity [4–6] the occurrence of a cavitation instability has been interpreted either as a bifurcation from a homogeneously stressed solid to a solid containing a void, or as the growth of a pre-existing void.

Rapid void growth under high stress triaxiality has been observed in experiments for Al_2O_3 reinforced by Al particles [7] and in experiments for a lead wire well bonded to a thick outer glass cylinder [8]. The cavitation in the constrained lead wire has recently been analysed by Tvergaard [9]. In a thin ductile metal layer bonding two ceramic blocks, constrained plastic flow tends to promote rapid void growth [10], and analyses for such cases, using remeshing techniques, have been able to follow the unstable growth through void volume increases by a factor of up to 10^{10} [11,12]. When the void radius is sufficiently small, the behaviour is not well described by conventional plasticity theory, and the material model must account for observed size-effects [13,14]). The effect of such size-effects on cavitation instabilities has recently been analysed by Niordson and Tvergaard [15].

The analyses of cavitation instabilities have assumed that there is only one void in an infinite solid or that void spacing compared to void size is so large that the average void volume fraction is essentially zero. But metals will

*Corresponding author. Fax: +45 45931475.
E mail address: viggo@mek.dtu.dk (V. Tvergaard).

often contain a distribution of micro voids, and it is of interest to find out how surrounding voids affect the occurrence of a cavitation instability at one of the voids. Analyses for a unit cell model containing two voids of different size have focussed on the amplification of the stress levels at a small void due to larger neighbouring voids [16,17]. In the present paper, the effect of void interaction is studied by analysing a unit cell model with a single central void discretely represented and with other voids represented by using the generalized Gurson model [18,19] for the metal surrounding the central void. Cases where the porosity is present from the beginning are analysed, as well as cases where the voids in the surrounding material nucleate gradually.

2. Problem formulation

Analyses are carried out for the growth of a single void in the centre of an infinite solid, where the nucleation and growth of other voids in the surrounding matrix is accounted for. A cylindrical unit cell model is used, where x^1 represents the axial coordinate, x^2 the radial coordinate and x^3 the circumferential angle in the reference coordinate system. Finite strains are accounted for. The initial dimensions of the unit cell have the values R_0 and R_i for the outer radius of the cylinder and the radius of the internal void, respectively, and also the value of R_0 for the height of the cell in axial direction. The boundary conditions assumed at the cell are as follows:

$$\dot{u}^1 = 0, \quad \dot{T}^2 = \dot{T}^3 = 0 \quad \text{at } x^1 = 0, \tag{2.1}$$

$$\dot{u}^1 = \dot{U}_{\mathrm{I}}, \quad \dot{T}^2 = \dot{T}^3 = 0 \quad \text{at } x^1 = R_0, \tag{2.2}$$

$$\dot{u}^2 = \dot{U}_{\mathrm{II}}, \quad \dot{T}^1 = \dot{T}^3 = 0 \quad \text{at } x^2 = R_0, \tag{2.3}$$

$$\dot{T}^i = 0 \quad \text{at } (x^1)^2 + (x^2)^2 = R_i^2. \tag{2.4}$$

The two constants $\dot{U}_{\mathrm{I}}$ and $\dot{U}_{\mathrm{II}}$ are displacements increments and the ratio $\dot{U}_{\mathrm{II}}/\dot{U}_{\mathrm{I}}$ is calculated in each increment such that there is a fixed prescribed ratio $\rho = T/S$, between the macroscopic true stresses [21]. Here, S is the average true stress in the axial direction, while T is the average true stress in the radial direction.

To describe the matrix material, an isotropic hardening plasticity model for a porous ductile material [18] is used, with a yield condition of the form $\Phi(\sigma^{ij},\ \sigma_M,\ f) = 0$. Here, σ^{ij} is the average macroscopic Cauchy stress tensor, σ_M is an equivalent tensile flow stress representing the actual microscopic stress-state in the matrix material and f is the current void volume fraction.

The approximate yield condition applied here is

$$\Phi = \frac{\sigma_e^2}{\sigma_M^2} + 2q_1 f \cosh\left(\frac{q_2}{2}\frac{\sigma_k^k}{\sigma_M}\right) - \left[1 + (q_1 f)^2\right] = 0, \tag{2.5}$$

where $\sigma_e = (3s_{ij}s^{ij}/2)^{1/2}$ is the macroscopic effective Mises stress, $s^{ij} = \sigma^{ij} - G^{ij}\sigma_k^k/3$ is the stress deviator, and $q_1 = q_2 = 1$ according to [18]. This approximation can be improved, as suggested in [20,21], by using the values $q_1 = 1.5$ and $q_2 = 1$.

To model the effect of coalescence, Tvergaard and Needleman [22] have suggested replacing the value of f by the function $f^*(f)$ of the form

$$f^*(f) = \begin{cases} f & \text{for } f \leqslant f_C, \\ f_C + \frac{f_U^* - f_C}{f_F - f_C}(f - f_C) & \text{for } f > f_C, \end{cases} \tag{2.6}$$

where $f_U^* = f^*(f_F)$ with the value $f_U^* = 1/q_1$. The chosen values of $f_C = 0.15$ and $f_F = 0.25$ are based on experimental results and on numerical model analyses.

Assuming that the rate of equivalent plastic work in the matrix material is equal to the macroscopic plastic work, it follows that

$$\sigma^{ij}\dot{\eta}_{ij}^P = (1-f)\sigma_M\dot{\varepsilon}_M^P. \tag{2.7}$$

Here, $\dot{\eta}_{ij}^P$ is the plastic part of the macroscopic strain rate, and the relation between $\dot{\varepsilon}_M^P$ and $\dot{\sigma}_M$ is taken to be

$$\dot{\varepsilon}_M^P = \left(\frac{1}{E_t} - \frac{1}{E}\right)\dot{\sigma}_M, \tag{2.8}$$

where E is Young's modulus and E_t is the slope of the uniaxial true stress-natural strain curve at the value σ_M. This curve is represented by a piecewise power law

$$\varepsilon = \begin{cases} \frac{\sigma}{E} & \sigma \leqslant \sigma_Y, \\ \frac{\sigma_Y}{E}\left(\frac{\sigma}{\sigma_Y}\right)^{1/N} & \sigma > \sigma_Y, \end{cases} \tag{2.9}$$

where σ_Y and N are the uniaxial yield stress and the strain hardening exponent of the matrix material, respectively.

The change of the void volume fraction during an increment of deformation is due to the effect of growth (first term) and nucleation (second and third term), and takes the form [23]

$$\dot{f} = (1-f)G^{ij}\dot{\eta}_{ij}^P + A\dot{\sigma}_M + B\left(\sigma_k^k\right)^{\bullet}/3. \tag{2.10}$$

Here, A and B have different values for strain-controlled nucleation and stress-controlled nucleation. For strain controlled nucleation, to be applied here, Chu and Needleman [24] have proposed the expression

$$A = \left(\frac{1}{E_t} - \frac{1}{E}\right)\frac{f_N}{s\sqrt{2\pi}}\exp\left[-\frac{1}{2}\left(\frac{\varepsilon_M^P - \varepsilon_N}{s}\right)^2\right], \quad B = 0 \tag{2.11}$$

corresponding to a normal distribution, where ε_N is the mean strain for nucleation, s is the standard deviation, and f_N is the value of the void volume fraction of the nucleating particles.

The plastic part of the macroscopic strain-rate for the porous material, is given by the expression

$$\dot{\eta}_{ij}^P = \frac{1}{H}m_{ij}^G m_{kl}^F \overset{\nabla}{\sigma}{}^{kl}, \tag{2.12}$$

where $\overset{\nabla}{\sigma}{}^{kl}$ is the Jaumann rate of the Cauchy stress. The values for H, m_{ij}^G and m_{ij}^F are given in [19]. For time-independent plasticity, the incremental stress–strain relationship is of the form $\dot{\tau}^{ij} = L^{ijkl}\dot{\eta}_{kl}$, where L^{ijkl} are the instantaneous moduli. Plastic yielding starts when $\Phi = 0$ and $\dot{\Phi} > 0$ during elastic deformation, and continued plastic loading requires $\Phi = 0$ and $m_{kl}^F \overset{\nabla}{\sigma}{}^{kl}/H \geqslant 0$.

For the finite strain analyses, a Lagrangian convected coordinate formulation of the field equations is adopted. In this formulation, a material point is identified in the reference configuration by x^i. The contravariant components of the Cauchy stress tensor σ^{ij} and the Kirchhoff stress tensor τ^{ij} are related by $\tau^{ij} = \sqrt{G/g}\sigma^{ij}$. The metric tensors in the current and the reference configuration are denoted by G_{ij} and g_{ij}, with the determinants G and g, respectively.

The dependence of elastic properties on porosity is usually not included in the generalized Gurson model. For an elastic solid containing the volume fraction f of spherical holes, Tandon and Weng [25] have derived the following relations for the macroscopic E and v, expressed in terms of the matrix values E_0 and v_0

$$E = \frac{2E_0(7-5v_0)(1-f)}{14-10v_0+f(1+v_0)(13-15v_0)},$$
$$v = \frac{v_0(14-10v_0)+f(1+v_0)(3-5v_0)}{14-10v_0+f(1+v_0)(13-15v_0)}. \tag{2.13}$$

Fleck et al. [26] suggested a simple linear dependence on f

$$E = E_0(\hat{f}-f)/\hat{f}, \quad v = v_0(\hat{f}-f)/\hat{f}. \tag{2.14}$$

The value of $\hat{f}$ recommended in Ref. [26] is $\hat{f} = 0.36$, corresponding to the limit of dense random packing of a sintered powder. For structural alloys a sintered powder is not relevant, and it seems more realistic to use $\hat{f} = 1/q_1 = 0.66$.

3. Numerical method

The Lagrangian strain tensor is given in terms of the displacement components u^i on the reference base vectors by

$$\eta_{ij} = \frac{1}{2}\left(u_{i,j} + u_{j,i} + u_{,i}^k u_{k,j}\right), \tag{3.1}$$

where $(\ )_{,j}$ denotes covariant differentiation in the reference frame.

The equilibrium equations are written in terms of the principle of virtual work. A numerical solution is obtained by a linear incremental solution procedure, by expanding the principle of virtual work about the current state, e.g. [19].The incremental equation is, to lowest order, equal to

$$\int_V \left\{\Delta\tau^{ij}\delta\eta_{ij} + \tau^{ij}\Delta u_{,i}^k \delta u_{k,j}\right\} \mathrm{d}V = \int_A \Delta T^i \delta u_i \,\mathrm{d}A - \left[\int_V \tau^{ij}\delta\eta_{ij}\,\mathrm{d}V - \int_A T^i \delta u_i \,\mathrm{d}A\right]. \tag{3.2}$$

Here, V and A are, respectively, the volume and surface of the body in the reference configuration, $\Delta\tau^{ij}$ and $\Delta\eta_{ij}$ are the stress and strain increments, T^i are contravariant components of the nominal surface tractions, etc. The bracketed terms are equilibrium corrections.

The displacement fields are approximated in terms of axisymmetric triangular elements, arranged in quadrilaterals of crossed triangles. There are 53 quadrilaterals in the radial direction, and 12 quadrilaterals in the circumferencial direction. The volume integral in Eq. (3.2) is carried out by using one integration point within each triangular element. Fig. 1 illustrates both the outer mesh in the unit cell and the central part of the mesh near a spherical void.

To improve the numerical stability when the occurrence of a cavitation instability is close, a special Rayleigh–Ritz finite element method [27] is used. This method make it possible to prescribe node displacements on the void surface without applying a load, rather than prescribing the end displacement of the unit cell.

Final ductile failure, when f reaches f_F in Eq. (2.6), has been represented in several papers in terms of an element vanish technique. Instead, we here use a small yield surface technique. In this method, it is chosen to use Eq. (2.6) in void growth predictions until $f^*(f) = 0.9f_U^*$ or $f^*(f) = 0.99f_U^*$ depending on the case, and after that keep the value of f constant.

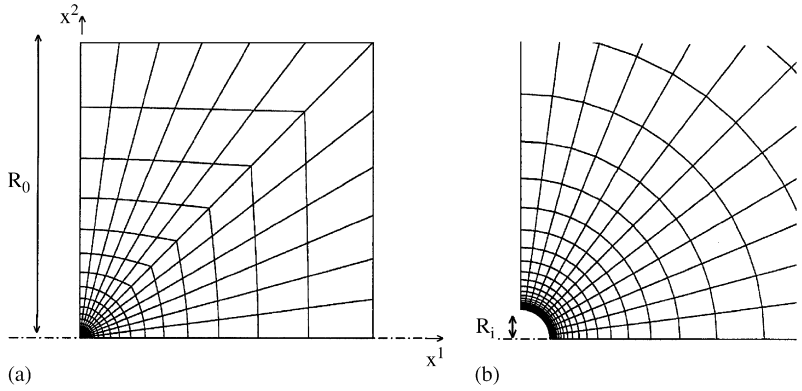

Fig. 1. Mesh used for numerical analyses: (a) The axisymmetric unit cell. (b) Inner mesh near the central void (magnified by factor 300).

4. Results

In the cell model analyses the ratio of the initial void radius to the outer radius of the cylinder is $R_i/R_o = 1/3000$, so that the void volume fraction corresponding to the central void alone is extremely small, 2.5×10^{-11}. The values of the material parameters are taken to be $\sigma_Y/E = 0.003$ and $\nu = 0.3$, with the power hardening exponent $N = 0.1$ in most of the cases. The value of the initial void volume fraction, f_o, or of the nucleation parameters, will be different for each case analysed.

First the effect of accounting for the porosity in the elastic properties is studied, by using the expressions (2.13) or (2.14) in the generalized Gurson model. For a very high initial void volume fraction, $f_o = 0.1$, with the macroscopic stress ratio $\rho = T/S = 0.9$ and $N = 0.1$, Fig. 2 shows a comparison of the normalized axial stress S/σ_Y vs. void volume V/V_o for the generalized Gurson model with no elasticity modification or with the modification (2.13) from Tandon and Weng. This high value of f_o is far above realistic values for porosity levels in structural metals, but could be relevant for powder compacted metals, as those studied in [26]. Even at this high value of f_o the stress level in Fig. 2 is only reduced by 1.9% when using the modification (2.13), and a similar comparison for $f_o = 0.01$ has shown a smaller difference of only 0.2%. Also the modification (2.14) has been tried, and it has been found that for $\hat{f} = 0.66$ the effect is similar to that of (2.13). For (2.14) with $\hat{f} = 0.36$ the reduction is a little bigger, 3.0% for the case presented in Fig. 2 with $f_o = 0.1$, but still quite small. In all the following computations, the modification (2.13) is applied, even though these comparisons have shown that the influence on the stress levels obtained is small.

Fig. 3 shows the influence of various levels of initial void volume fraction in the matrix material, for the stress ratio $\rho = 0.9$ and strain hardening exponent $N = 0.1$, as in Fig. 2. No void nucleation is included in these studies. For

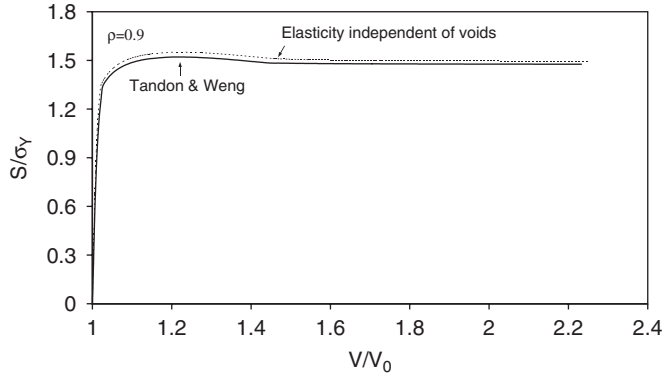

Fig. 2. Computation accounting for reduced elastic stiffness due to voids, compared to result of traditional porous material model. The initial void volume fraction is high, $f_o = 0.1$, relevant only to a sintered metal powder. Furthermore, $\rho = 0.9$ and $N = 0.1$.

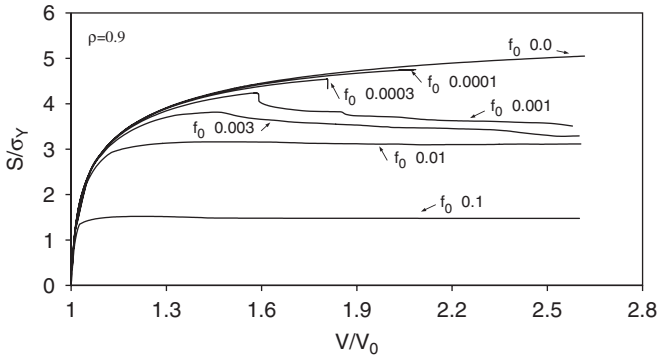

Fig. 3. Influence of various levels of initial void volume fraction, f_o, for $\rho = 0.9$ and $N = 0.1$, when there is no void nucleation.

comparison, the programme has also been used to calculate the curve for $f \equiv 0$, as shown in the figure. This computation has been continued up to $V/V_o = 40.7$, and the stress level found at this point is $S/\sigma_Y = 5.681$, which is in good agreement with the cavitation instability limit determined in [3]. The curves for the values 0.0001, 0.0003, 0.001, 0.003, 0.01 and 0.1 of the initial void volume fraction f_o show that the level of the maximum stress is significantly reduced by the presence of voids in the material surrounding the central void. Thus, for the small value $f_o = 0.0003$ the maximum stress is reduced noticeably, to $S/\sigma_Y = 4.540$. The curve for this small value of f_o actually follows closely along that for $f \equiv 0$, but then the maximum is reached already at $V/V_o = 1.81$, so that the stress never gets near the cavitation instability level corresponding to $f \equiv 0$. At this stage the macroscopic stress drops rapidly for nearly constant value of V/V_o, and the computation is so unstable that it is difficult to continue. This behaviour is also found for $f_o = 0.0001$ in Fig. 3, but with stronger numerical instability so that the downward part of the curve after the maximum is not visible in the figure.

To further investigate the type of behaviour found for $f_o = 0.0003$, the very similar rapid stress drop found for $f_o = 0.001$ in Fig. 3 is investigated. Just before the rapid load drop, at $V/V_o = 1.59$, the void volume fractions along the surface of the central void have grown to $f = 0.002$, but a slightly larger void volume fraction of $f = 0.003$ is developing along a spherical surface at a distance of about 4.5 R_i outside the current surface of the central void. Then, suddenly, near this spherical surface, at the symmetry plane $x^1 = 0$, the void volume fraction starts to grow rapidly, and this growth seems to result in the sudden stress drop seen in Fig. 3. After the load drop the voids keep growing locally in this region, and Fig. 4 shows a plot of the void volume fraction contours in the current configuration at $V/V_o = 1.76$, where the peak value has reached $f \approx 0.04$. For $f_o = 0.003$ in Fig. 3 the behaviour at the load maximum is somewhat similar to that for $f_o = 0.001$, but the load drop is less abrupt.

Fig. 5 shows similar curves as those in Fig. 3, but now for $\rho = 1.0$. Here, for $f_o = 0.001$ there is a sudden small load reduction at $V/V_o = 2.54$, which is rather analogous

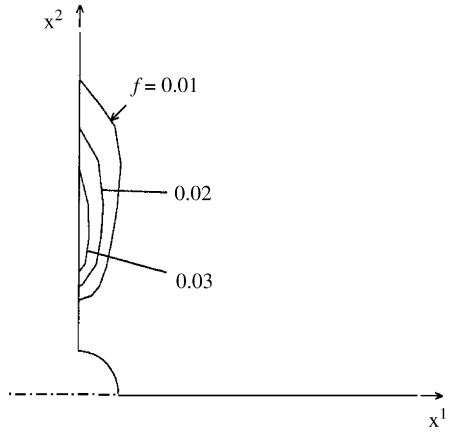

Fig. 4. Contours of constant void volume fraction at the stage where $V/V_o = 1.76$, for the computation with $f_o = 0.001$, $\rho = 0.9$ and $N = 0.1$. The contours show the formation of a toroidal region of increased porosity near the symmetry plane $x^1 = 0$.

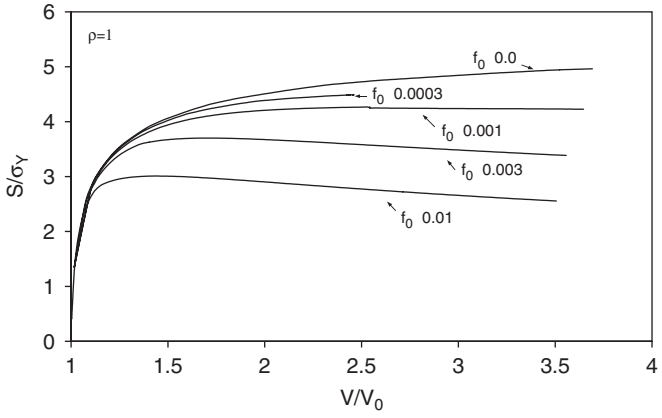

Fig. 5. Influence of various levels of initial void volume fraction, f_o, for $\rho = 1.0$ and $N = 0.1$, when there is no void nucleation.

to that illustrated in Figs. 3 and 4 for $f_o = 0.001$. Just before the load drop, a uniformly increased void volume fraction has developed along a spherical surface a few void radii outside the central void. If the cell model for this case of pure hydrostatic tension had full spherical symmetry, a bifurcation would be necessary in order that the increased void volume fraction along the spherical surface could begin to deviate from spherical symmetry. However, here the cylindrical shape of the cell model represents a small imperfection, which triggers the sudden development of a locally increased void volume fraction much like the distribution shown in Fig. 3, but in this case located at the x^1 axis. For the smallest value of the void volume fraction analysed, $f_o = 0.0003$, the computation stopped due to strong numerical instability. It is possible that the stress maximum has not quite been reached at this point, but it is expected that the end value of the stress still gives a good indication of the maximum level. For the two larger values of f_o in Fig. 5 there is a rather smooth decay of the load after the maximum, and here the increased void volume fraction at some distance outside the central void remains close to a spherical surface, as f grows larger.

Curves of maximum stress values as a function of $\rho = T/S$ are shown in Fig. 6. It is seen that in the range analysed, for $1.0 \leqslant \rho \leqslant 0.85$, the reduction in the maximum stress below the cavitation stress corresponding to $f \equiv 0$ varies continuously as a function of ρ. The curves in Fig. 6 are based on the maximum values determined in Figs. 3 and 5, and on similar figures calculated for $\rho = 0.95$ and for $\rho = 0.85$, which are not shown here.

For cases where the initial void volume fraction is zero, $f_o = 0$, but where voids nucleate according to a strain controlled rule (2.11), curves of S/σ_Y vs. V/V_o are shown in Fig. 7, for $\rho = 0.9$ and $N = 0.1$. Here, of course, the effect of elasticity modifications such as (2.13) or (2.14) is much smaller than that in the previous figures, since the void volume fraction is zero everywhere, except for a small region in the near vicinity of the central void. For the mean nucleation strain $\varepsilon_N = 0.3$ curves are shown in Fig. 7 corresponding to two values of f_N, 0.03 and 0.01. In both cases the curves are rather close to that for $f \equiv 0$, but the maximum load levels are smaller, since the load maxima occur at values of V/V_o well below those reached for $f \equiv 0$. The curve for $f_N = 0.03$ and $\varepsilon_N = 0.15$ is below the other curves, and ends at a much smaller value of V/V_o, but is otherwise rather similar to the two other curves.

To consider the influence of hardening, a set of analyses for $N = 0.2$ have been shown in Fig. 8. These results are rather similar to those shown in Fig. 3, but the maximum values of S/σ_Y reached are higher in all cases, as expected due to the higher value of N. The curve for $f_o = 0.0001$ can here be followed a bit after the load maximum, but then the computation becomes numerically unstable. The computations corresponding to the other curves are less unstable than those in Fig. 3, and the curves decay smoothly after the load maximum.

As was mentioned in Section 2, final ductile failure is here represented numerically by the approximate procedure that when $f^* = r\, f^*(f_F)$ is reached, the value of f is subsequently kept constant, so that in fact the failed material is represented as an elastic-plastic material with a

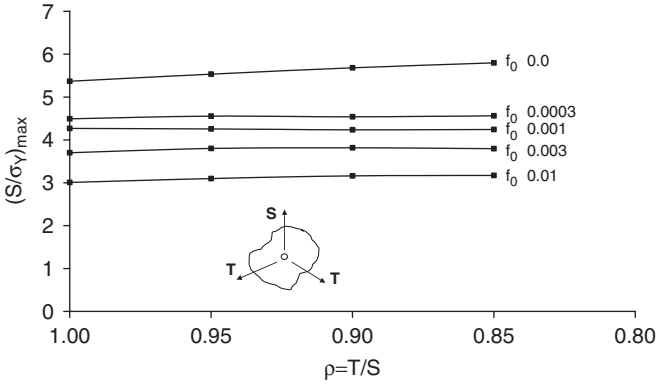

Fig. 6. Curves of maximum stress values vs. ρ for various levels of initial void volume fraction, f_o, and for $N = 0.1$. There is no void nucleation.

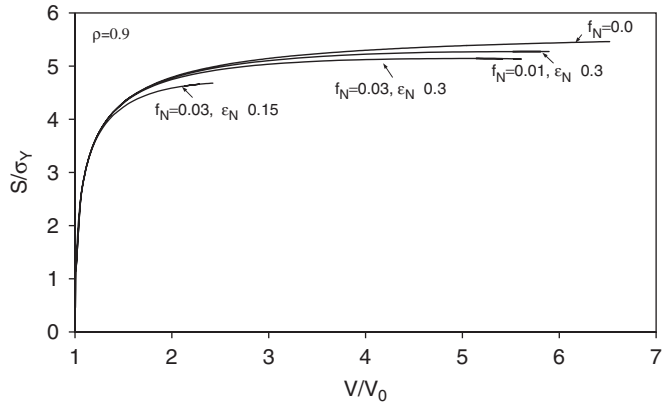

Fig. 7. Influence of plastic strain controlled nucleation according to (2.11), for $f_o = 0.0$, $\rho = 0.9$ and $N = 0.1$.

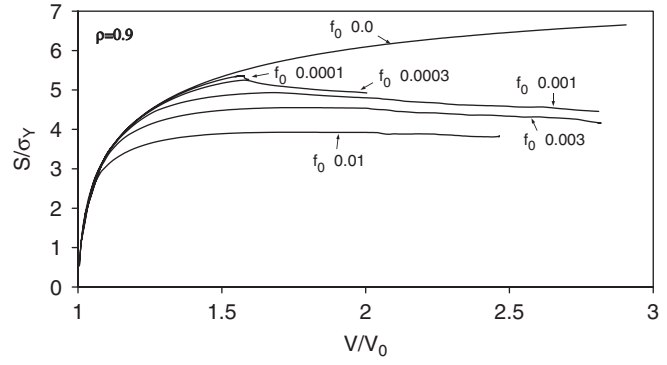

Fig. 8. Influence of various levels of initial void volume fraction, f_o, for $\rho = 0.9$ and $N = 0.2$, when there is no void nucleation.

very small yield stress. In most of the present computations $r = 0.9$ has been used, but values closer to unity have also been used in a few cases. In Fig. 8, the two curves for $f_o = 0.01$ and 0.003 showed the unexpected behaviour that the load started to slowly increase again after that the failure condition corresponding to $r = 0.9$ had been reached, at $V/V_o \approx 2.3$. The two curves shown in Fig. 8 have been recomputed using $r = 0.99$, and it is seen that this removed the tendency to increase S. Also in Fig. 3, where the failure condition for $f_o = 0.003$ was reached at $V/V_o \approx 2.0$, the curve shown has been computed for $r = 0.99$, and the end of the curve is slightly lower than that corresponding to $r = 0.9$. Clearly, using $r = 0.99$ in all cases would be more realistic, but is also numerically less stable, and has therefore only been done in a couple of cases.

5. Discussion

The idea of using a porous ductile material model to describe the matrix material between discrete voids was first introduced in [28], in order to analyse ductile failure mechanisms in a metal containing two populations of voids. The same type of idea has subsequently been used in a number of analyses of crack growth in ductile materials, as e.g. [29]. Recently, Enakoutsa et al. [30] have worked on a model that accounts for coupling between growth of big voids with the growth and coalescence of smaller voids in the surrounding matrix. The models used in the present study are similar to the previous ones, but here the porosity in the material surrounding the central void is not necessarily used to represent smaller voids. Here the porosity is used to estimate the influence of a distribution of other voids of perhaps the same size located at some distance from the central void in the cell model.

The focus here is on high triaxiality cases with $\rho \approx 1$, where unstable cavity growth tends to occur. But it is noted that for much lower values of ρ, as those considered in [28], the dominant mode of instability will involve the occurrence of shear bands by the interaction of the different populations of voids.

Since unstable cavity growth in an infinite solid is driven by the stored elastic energy in the body, the reduction in elastic energy due to porosity could be important. Therefore, the reductions of Young's modulus and Poisson's ratio due to porosity have been included in the present analyses in an approximate manner. However, it has been found that even for a large porosity (as $f_o = 0.1$ in Fig. 2), the effect is small. For lower levels of the void volume fraction, more realistic in structural metals, the difference is even less relevant. Although the porosity effect is small, elastic constants dependent of f (Eq. (2.13)) are used for all the computations done.

The effect found from porosity around a central void is that, with initial porosity but no nucleation, the level of the maximum stress is significantly reduced compared to that in the absence of any porosity, even for small values of f_o. This reduction is higher if the value of f_o is increased. The sudden stress drop that appears in some cases in Figs. 3 and 5 are due to the local growth of the void volume fraction in regions outside the current surface of the central void. Results also show that with higher values of N (more strain hardening), higher values of the maximum stress are found. With strain controlled nucleation, but without an initial void volume fraction, there is not a strong effect on the maximum stress levels reached.

In a real material, the voids surrounding our central void will be discrete voids with their centres located at particular points, and the predictions would depend on where these locations are. Thus, in the case corresponding to the contour curves shown in Fig. 4, the predictions will be relevant to situations where some voids are located inside or near the toroidal region shown as a higher porosity region in the figure, but if there are no voids in this vicinity, the sudden load decay observed in Fig. 3 for $f_0 = 0.001$ cannot be expected to happen. However, some similar behaviour would be expected with some delay when the discrete voids first activated in the surrounding matrix material are located at some distance from the higher porosity region shown in Fig. 4. Analogous comments apply to curves for $\rho = 1$ (Fig. 5), where a high porosity

region is predicted at the x^1 axis, or along a spherical surface outside the central void.

The results found here show some similarity with those found in [15], in the sense that a maximum value of the remote stress is reached while the value of V/V_o is still quite small, and that the void subsequently grows large while the remote stress level is somewhat below the maximum. In [15] this is a result of material length scales dependent on dislocation spacings, where void growth is slower while the void radius is comparable to the characteristic material length, but where this effect is reduced as the void grows larger than the material length. In the present analyses the early stress maximum is reached due to the damage evolution in the material adjacent to the central void, and the lower stress level during the subsequent growth of the central void results from progressive damage evolution during the void growth.

References

[1] Bishop RF, Hill R, Mott NF. The theory of indentation and hardness tests. Proceedings of the Physical Society 1945;57:147 59.

[2] Huang Y, Hutchinson JW, Tvergaard V. Cavitation instabilities in elastic plastic solids. Journal of Mechanical Physics and Solids 1991;39:223 41.

[3] Tvergaard V, Huang Y, Hutchinson JW. Cavitation instabilities in a power hardening elastic plastic solid. European Journal of Mechanics A/Solids 1992;11:215 31.

[4] Ball JM. Discontinuous equilibrium solutions and cavitation in nonlinear elasticity. Philosophical Transaction of the Royal Society of London A 1982;306:557 610.

[5] Horgan CO, Abeyaratne R. A bifurcation problem for a compressible nonlinearly elastic medium: growth of a microvoid. Journal of Elasticity 1986;16:189 200.

[6] Horgan CO, Polignone DA. Cavitation in nonlinearly elastic solids: a review. Applied Mechanics Reviews 1995;48:471 85.

[7] Flinn B, Ruhle M, Evans AG. Toughening in composites of Al_2O_3 reinforced with Al. Materials Department report, University of California, Santa Barbara, 1989.

[8] Ashby MF, Blunt FJ, Bannister M. Flow characteristics of highly constrained metal wires. Acta Metallurgica 1989;37:1847 57.

[9] Tvergaard V. Effect of residual stress on cavitation instabilities in constrained metal wires. Transactions of the ASME. Journal of Applied Mechanics 2004;71:560 6.

[10] Dalgleish BJ, Trumble KP, Evans AG. The strength and fracture of alumina bonded with aluminum alloys. Acta Metallurgica 1989;37:1923 31.

[11] Tvergaard V. Studies of void growth in a thin ductile layer between ceramics. Computational Mechanics 1997;20:186 91.

[12] Tvergaard V. Interface failure by cavity growth to coalescence. International Journal of Mechanical Sciences 2000;42:381 95.

[13] Fleck NA, Hutchinson JW. Strain gradient plasticity, Advances in applied mechanics. New York: Academic Press; 1997.

[14] Stolken JS, Evans A. A microbend test method for measuring the plasticity length scale. Acta Materialia 1998;46:5109 15.

[15] Niordson CF, Tvergaard V. Size effects on cavitation instabilities. Report 2005, Department of Mechanical Engineering, Solid Mechanics, Technical University of Denmark.

[16] Tvergaard V. Interaction of very small voids with larger voids. International Journal of Solids Structures 1998;35:3989 4000.

[17] Tvergaard V, Niordson CF. Nonlocal plasticity effects on interaction of different size voids. International Journal of Plasticity 2004;20:107 20.

[18] Gurson AL. Continuum theory of ductile rupture by void nucleation and growth I. Yield criteria and flow rules for porous ductile media. Journal of Engineering Materials and Technology 1997;99:2 15.

[19] Tvergaard V. Material failure by void growth to coalescence. Advances in Applied Mechanics 1990;27:83 151.

[20] Tvergaard V. Influence of voids on shear band instabilities under plane strain conditions. International Journal of Fracture 1981;17:389 407.

[21] Tvergaard V. On localization in ductile materials containing spherical voids. International Journal of Fracture 1982;18:237 52.

[22] Tvergaard V, Needleman A. Analysis of the cup cone fracture in a round tensile bar. Acta Metallurgica 1984;32:157 69.

[23] Needleman A, Rice JR. Limits to ductility set by plastic flow localization. Mechanics of sheet metal forming. New York: Plenum Publishing; 1978.

[24] Chu CC, Needleman A. Void nucleation effects in biaxially stretched sheets. Journal of Engineering Materials and Technology 1980;102:249 56.

[25] Tandon GP, Weng GJ. A Theory of particle reinforced plasticity. Transactions of the ASME. Journal of Applied Mechanics 1988;55:126 35.

[26] Fleck NA, Otoyo H, Needleman A. Indentation of porous solids. International Journal of Solids Structures 1992;29:1613 36.

[27] Tvergaard V. Effect of thickness inhomogeneities in internally pressurized elastic plastic spherical shells. Journal of Mechanics and Physics of Solids 1976;24:291 304.

[28] Tvergaard V. Ductile fracture by cavity nucleation between larger voids. Journal of Mechanics and Physics of Solids 1982;30:265 86.

[29] Tvergaard V, Needleman A. Effect of crack meandering on dynamic, ductile fracture. Journal of Mechanics and Physics of Solids 1992;40:447 71.

[30] Enakoutsa K, Leblond J B, Audoly B. Influence of continuous nucleation of secondary voids upon growth and coalescence of cavities in porous ductile metals. In: Proceedings of ICF11, Turin, Italy, 20 25 March 2005 (on CD).